Unraveling a Ligand-Induced Twist of a Homodimeric Enzyme by Pulsed Electron–Electron Double Resonance

Dzung Nguyen+, Dinar Abdullin+, Caspar A. Heubach, Toni Pfaffeneder, Andreas Nguyen, Andreas Heine, Klaus Reuter, François Diederich†, Olav Schiemann,* and Gerhard Klebe*

Abstract: *Mechanistic insights into protein–ligand interactions can yield chemical tools for modulating protein function and enable their use for therapeutic purposes. For the homodimeric enzyme tRNA-guanine transglycosylase (TGT), a putative virulence target of shigellosis, ligand binding has been shown by crystallography to transform the functional dimer geometry into an incompetent twisted one. However, crystallographic observation of both end states does neither verify the ligand-induced transformation of one dimer into the other in solution nor does it shed light on the underlying transformation mechanism. We addressed these questions in an approach that combines site-directed spin labeling (SDSL) with distance measurements based on pulsed electron–electron double resonance (PELDOR or DEER) spectroscopy. We observed an equilibrium between the functional and twisted dimer that depends on the type of ligand, with a pyranose-substituted ligand being the most potent one in shifting the equilibrium toward the twisted dimer. Our experiments suggest a dissociation–association mechanism for the formation of the twisted dimer upon ligand binding.*

Introduction

A large number of proteins undergoes a carefully arranged interplay with other macromolecules to perform biological functions. Self-association into oligomeric states via protein–protein interactions (PPIs) represents one option for the functional regulation of proteins i.e., specific enzymes can accomplish their catalysis only in a homo-oligomeric arrangement.[1–3] Disturbing and preventing this oligomerization with small molecules and peptides/peptidomimetics is therefore a promising concept to modulate and inhibit the function of such enzymes, as shown for the dimeric Kaposi's sarcoma-associated herpesvirus protease.[4,5] However, less exploited strategies such as transferring or stabilizing a protein in a non-functional oligomeric state also represent an attractive approach for drug design. This concept has been exemplified by the development of the small molecule BI-2852 that successfully stabilizes a non-functional dimeric form of KRAS, a member of the GTPase protein family and the most frequently mutated proto-oncogene in human cancers.[6] Another example is the discovery of orthosteric PPI stabilizers for the dimeric N-terminal domain of the MERS-CoV nucleocapsid protein, which demonstrated that the stabilization of non-native PPIs could serve as targets for the design of novel antiviral drugs.[7]

Recently, we discovered a ligand-induced structural rearrangement of the homodimeric tRNA-modifying enzyme tRNA-guanine transglycosylase (TGT) (Figure 1 a).[8,9] This bacterial enzyme is involved in catalyzing a complete nucleobase exchange reaction at the wobble position of specific tRNA molecules. Although both monomeric subunits of TGT each contain a catalytic site, the enzyme can only recognize its tRNA substrate as a homodimer and binds only one substrate molecule per homodimer.[10,11] Binding of ligands with a *lin*-benzoguanine scaffold (Figure 1 b), specifically substituted in the 4-position, led to the formation of a novel twisted arrangement of the TGT dimer.[9] Surprisingly, the ligand-bound TGT crystallized side-by-side in both dimeric states i.e., the functional and the twisted, from the same crystallization well (Figure 1 a). We hypothesized that the twisted dimer is unable to bind and process the tRNA substrates for steric reasons, rendering the enzyme inactive in this state. With respect to drug discovery, ligands that initiate and stabilize the inactive twisted form could thus represent potential inhibitors of this enzyme. However, the crystal structures mark the end-points of the transformation but do not provide insights whether this transformation is indeed carried out dynamically in solution and what the underlying mechanisms are.

Pulsed electron–electron double resonance (PELDOR or DEER)[12,13] in combination with site-directed spin labeling (SDSL)[14] is a powerful method to study conformational changes in proteins.[15–21] In SDSL, spin labels are site-

[*] D. Nguyen,[+] A. Nguyen, A. Heine, K. Reuter, G. Klebe
Institut für Pharmazeutische Chemie, Philipps-Universität Marburg
Marbacher Weg 8, 35032 Marburg (Germany)
E-mail: klebe@mailer.uni-marburg.de

D. Abdullin,[+] C. A. Heubach, O. Schiemann
Institute of Physical and Theoretical Chemistry, University of Bonn
Wegelerstr. 12, 53115 Bonn (Germany)
E-mail: schiemann@pc.uni-bonn.de

T. Pfaffeneder, F. Diederich
Laboratorium für Organische Chemie, ETH Zürich
Vladimir-Prelog-Weg 3, HCI, 8093 Zürich (Switzerland)

[+] These authors contributed equally to this work.

[†] deceased

Supporting information and the ORCID identification number(s) for the author(s) of this article can be found under:
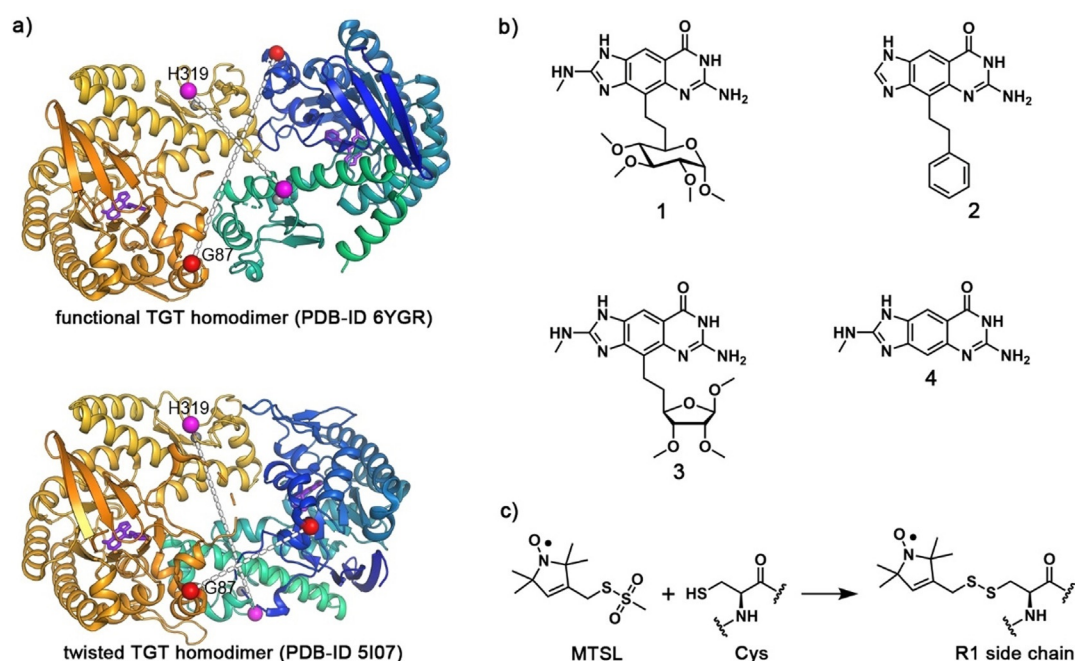https://doi.org/10.1002/anie.202108179.

Figure 1. a) The spin-labeling sites in TGT(G87R1) (red spheres) and TGT(H319R1) (magenta spheres) are shown together with the crystal structures of the functional (top) and twisted (bottom) TGT homodimers. The protein structure is displayed as a cartoon model. Zinc ions are shown as grey spheres. Ligand **2** is shown as a purple stick model. White dashed lines connect the spin-labeling sites, between which the PELDOR-based distance measurements were carried out. b) The chemical structures of ligands **1–4**. c) Bioconjugation of MTSL to a cysteine residue resulting in the R1 side chain.

specifically attached to the protein. Most commonly, the methanethiosulfonate spin label (MTSL)[22,23] is used, which reacts selectively with the thiol group of cysteines forming the so-called R1 side chain containing a disulfide linkage (Figure 1c). Site specificity is achieved by mutating cysteines into the protein sequence at the desired positions and mutating unwanted cysteines to, for example, alanine or serine. In PELDOR, the dipolar coupling between two such spin labels is then measured and transformed into distance distributions,[24–27] where conformational changes mirror themselves as changes in the inter-label distributions.[28–31]

Here, we report on SDSL/PELDOR experiments to follow the kinetics of the ligand-induced transformation of the TGT dimer in solution. We therefore selected the inhibitors **1** and **2**, for which both forms have been characterized crystallographically, whereas with **3** and **4** only the functional form has yet been observed. On two variants, TGT(G87R1) and TGT(H319R1), we verify the formation of the twisted dimer upon ligand addition and quantify the ratio between the two dimer states over time and in dependence of the type of ligand (Figure 1). Additional PELDOR experiments on heterodimeric TGT mixtures enable the estimation of dimer-to-monomer ratios leading to two proposed mechanisms for the transformation of the functional into the twisted dimer state.

Results and Discussion

To enable PELDOR measurements, TGT was spin-labeled with MTSL (Figure 1c and SI, Chapter 1). Since

TGT is overwhelmingly a homodimer in solution,[11] the spin labeling of a single residue is sufficient to enable inter-monomer distance measurements. Availability of the crystal structures for both dimer states, the functional and the twisted, allowed the systematic search for the best spin-labeling sites using the in silico spin labeling program *MtsslWizard*.[32] This search was based on the following criteria: (1) The selected site has to be accessible for the spin label in both protein states, (2) the distance r between two spin-labeled sites should be in the range of 15–60 Å in both protein states, (3) r should differ between the functional and twisted states by more than 5 Å. The first criterion is necessary for obtaining good labeling efficiencies and minimizing structural perturbations in the protein by the R1 side chain. The second criterion ensures that the inter-nitroxide distances are within the PELDOR range. The third criterion allows for a clear differentiation between both dimer states in the distance distributions. The details of the *in silico* simulations and the full set of selected spin-labeling sites are given in the SI, Chapter 2. From this selected set of sites, we then chose two, namely 87 and 319, because in their cases the distance distributions are predicted to be well separated (Figure 1a). Each of these positions was mutated to a cysteine, yielding the variants G87C and H319C. To avoid formation of any unspecific modifications and intermolecular disulfide linkages, the conservative mutations C158S and C281S were introduced into both variants. Then, both variants were spin-labeled with MTSL at the introduced cysteines yielding TGT(G87R1) and TGT(H319R1). Kinetic characterization showed no decrease in the enzymatic activity of the spin-labeled variants compared to the wild-type (WT) enzyme (SI,

Chapter 1.4). Moreover, to ensure that the introduced alterations in TGT did not significantly change the native homodimeric structure, both mutants were successfully crystallized in the functional state (SI, Chapters 1.5 and 1.6). Only marginal perturbations could be observed in the overall tertiary structure compared to that of the unlabeled WT dimer (Figure S3a). In case of TGT-(G87R1), no electron density was observed for the R1 spin label indicating high residual flexibility whereas in TGT-(H319R1), the spin label could be successfully resolved after initial refinement. Furthermore, the homodimeric states of both spin-labeled variants in solution were verified by gel filtration compared to homodimeric WT TGT and the mainly monomeric TGT(Y330D) mutant (Figure S3b).

PELDOR measurements (for details see SI, Chapter 3) were carried out for both variants, TGT(G87R1) and TGT-(H319R1), in the presence and absence of a ligand. Ligand-bound forms were obtained after incubation of each variant with either 3 equiv. of ligands **1–4** (Figure 1b) or 1.5 equiv. of tRNA for 24 h at room temperature. The amounts of added ligands were estimated to be sufficient to completely occupy the $preQ_1$ binding pockets of both TGT homodimer units.[9] The amount of added tRNA was chosen two times smaller than the amount of the ligands, because only one tRNA molecule binds to dimeric TGT. The results of the PELDOR measurements on the ligand-free and ligand-bound forms of TGT(G87R1) and TGT(H319R1) are depicted in Figure 2 and Figures S5–S7. As can be seen from Figure 2a, all PELDOR time traces have a good modulation depth of about 30%, a distinct dipolar oscillation, and an excellent signal-to-noise ratio (93 ± 24). This allowed accurate conversion of the primary PELDOR data into inter-nitroxide distance distributions using the Tikhonov regularization[26] (Figure 2b, rows 6–11, black distributions) and the *DEERNet* algorithm[25] as implemented in *DeerAnalysis* (Figures S6d and S7d), with both methods yielding very similar distance distributions. As can be seen from Figure 2b, row 6, the distance distribution for ligand-free TGT(G87R1) contains a single peak at around 54 Å, whereas the distance
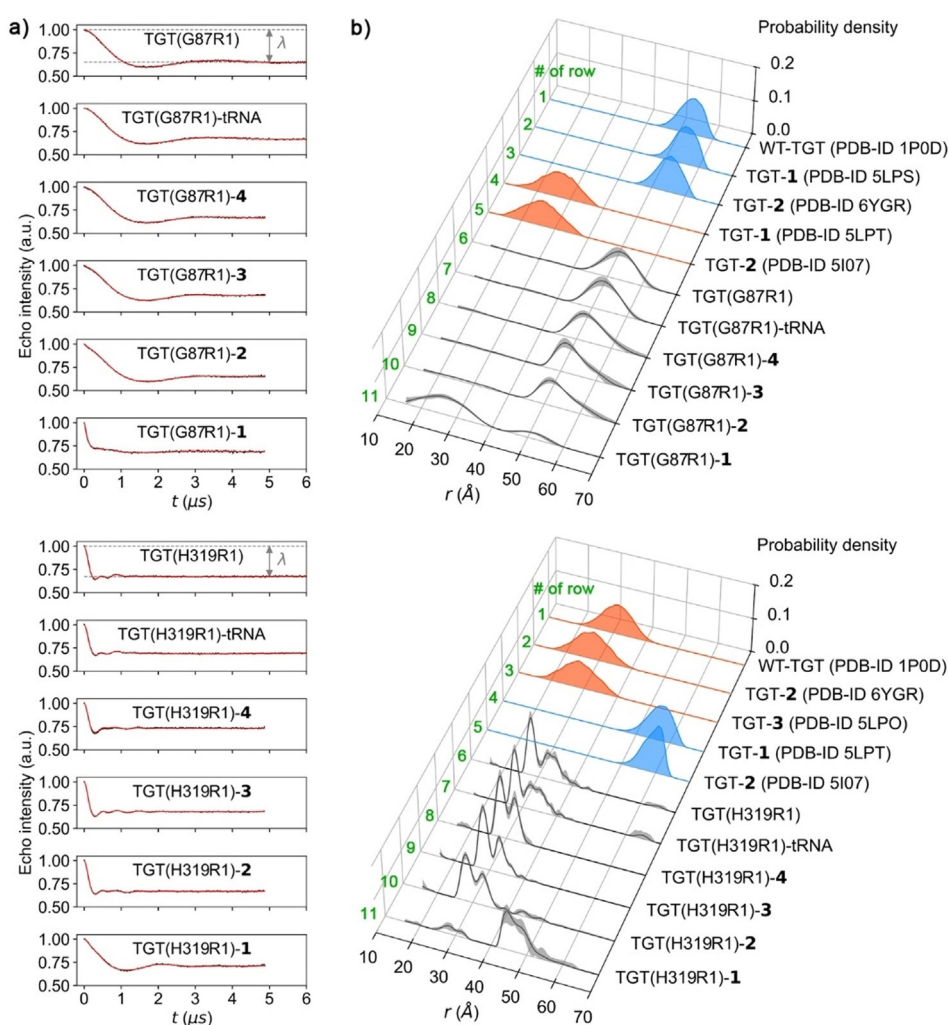

Figure 2. PELDOR measurements on TGT(G87R1) (top) and TGT(H319R1) (bottom) incubated over 24 h with the ligands **1–4** or tRNA. a) Background-corrected PELDOR time traces (black lines) and their fits (red lines). The original PELDOR time traces are given in Figures S5–S7. The gray arrow depicts the modulation depth parameter λ. b) PELDOR-based inter-nitroxide distance distributions (rows 6–11, black lines) and their in silico predictions based on the crystal structures of the twisted (rows 4–5, red shades) and functional (rows 1–3, blue shades) TGT homodimers. The error estimates for the PELDOR-derived distributions are shown as gray shades.

distribution of ligand-free TGT(H319R1) is bimodal with two maxima at around 28 Å and 34 Å. Most likely, the bimodality results from two different conformational ensembles of the spin label at position 319. Notably, the observed distance distributions of both variants in the ligand-free state (row 6) are in good agreement with the distance predictions obtained from the crystal structures of the functional TGT dimer (rows 1–3). This allows assigning the observed distance distributions for the ligand-free state to the functional state. A very similar assignment can also be made for the samples of TGT(G87R1) and TGT(H319R1) incubated with tRNA, (row 7) and ligands **4** (row 8) and **3** (row 9), as their distance distributions are within the error of the experiment unchanged compared to the ones of the ligand-free variants. In contrast, pronounced changes in the distance distributions are observed when both mutants are incubated with **1** (row 11). In addition to the distance peaks found for the ligand-free

variants, another peak appears at around 28 Å for TGT-(G87R1)-**1** and around 46 Å for TGT(H319R1)-**1**. Comparing with the distance predictions based on the crystal structures of the functional (blue) and twisted (red) TGT dimers (rows 1–3 and 4–5, respectively), the additional distance peaks can be assigned to the twisted dimer. Although this assignment is fairly straightforward for TGT(G87R1)-**1**, it is less obvious in the case of TGT(H319R1)-**1**. In the latter case, the experimental distance peak deviates from the prediction by 14 Å. This difference could be due to the structure of the twisted TGT dimer being locally different at site 319 in frozen solution and the crystalline state. Indeed, the crystal structure of the twisted dimer (PDB-ID 5LPT) reveals that the zinc-binding subdomain, which hosts the spin-labeled residue H319, is located rather closely to the adjacent crystal mate and, therefore, its orientation in the crystal might be influenced by the crystal packing forces. Finally, all distance peaks, which were identified for the TGT variants with bound **1**, are also observed for the corresponding TGT variants bound to **2**. However, the relative intensities of the peaks corresponding to the twisted dimer are significantly smaller in the case of **2** as compared to **1**. In order to quantify the relative amounts of functional and twisted dimers (Figure 2c), the integrals of the corresponding distance peaks were calculated for all TGT samples (see SI, Chapter 3.3). For TGT(G87R1), ligands **1** and **2** transform 82^{+7}_{-9}% and 12^{+7}_{-6}% of the functional dimer into the twisted dimer, respectively, and for TGT(H319R1) 84^{+10}_{-7}% and 8^{+14}_{-8}%, respectively (see also Table S4). Thus, both TGT variants yield similar amounts of twisted dimer for the same ligands.

To verify that the incubation time of 24 h was sufficient to reach the equilibrium, PELDOR measurements were repeated on ligand-bound samples of TGT(G87R1) equilibrated for 1, 24, and 72 h (Figures S8–S10). As can be seen in Figure 3, samples TGT(G87R1)-**1** and TGT(G87R1)-**2** appear to be fully equilibrated after 24 h, and no further increase of the relative amounts of twisted dimers is observed after 72 h. Figure 3 also reveals that, at least with **1**, the relative amounts of twisted dimers increase as the incubation time increases from 1 to 24 h. Given the fact that the conformational change

proceeds on a time scale of hours, diffusion-controlled ligand binding cannot be the rate-determining step. Therefore, the observed conversion rate must be related to a slow structural re-organization mechanism of the TGT dimers.

Importantly, Figures 2b and 3 reveal that the equilibrium state of the ligand-bound variants of TGT corresponds to a mixture of functional and twisted dimers. Moreover, the relative amounts of both dimers strongly depend on the type of the added ligand. This result is consistent with our previous crystallographic studies, which showed that both, the functional and the twisted dimers, can be crystallized from the same well with **1**.[9] With **2**, which populates less the twisted form in solution, we succeeded to obtain both forms only using separate crystallization trials. With **3** and **4**, where no evidence for the formation of the twisted form in solution has been found, up to present only the crystal form of the functional dimer could be obtained. To rationalize the latter findings in structural terms, the protein geometry around the ligand binding site was scrupulously examined using the available crystal structures of functional and twisted TGT dimers (Figure 4). First, it can be seen that the moieties of **1–3** are in close contact with hydrophobic residues V45, L68, and V282 at the bottom of the ribose-34 pocket. Consequently, the loop-helix motif, which shields the aromatic hotspot from water access, adopts a perturbed conformation in the ligand-bound functional as well as twisted dimer state (Figure 4a–c). Besides the structural rearrangement of the loop-helix motif, the structure of helix αA (residues G105–L111) was found to be influenced by the ligands (Figure 4a,b). In the case of **2** and **3** bound to the functional TGT dimer, helix αA adopts a similar conformation as in the *apo* structure. However, in the case of **1** bound to the functional dimer, this helix is not defined in the electron density, indicating higher residual mobility or scatter over multiple arrangements (Figure 4a). This can be explained by the steric conflict of residue Q107 with the anomeric methoxy group of the pyranose substituent of **1** that points toward helix αA (Figure 4a,d). Ligands **2** and **3** lack this sterically demanding group, allowing Q107 and helix αA to adopt a virtually unperturbed geometry. Thus, in addition to the collapse of the loop-helix motif, a destabiliza-

tion of helix αA might assist and lower the barrier for the formation of the twisted dimer. Note, that upon the formation of the twisted TGT dimer, helix αA undergoes structural rearrangements, leading to the formation of a new interface contact between residues Q107 and E339 via hydrogen bonds. Finally, the zinc-binding domain becomes increasingly destabilized when the functional TGT dimer is bound to ligand **1**. This is evidenced by the ill-defined residues E317–Q324 (Figure 4e) and a lower zinc occupancy (21%), as compared to the functional TGT homodimer bound to **2** and **3** (44% and 100%, respectively). The zinc-binding domain is located in the
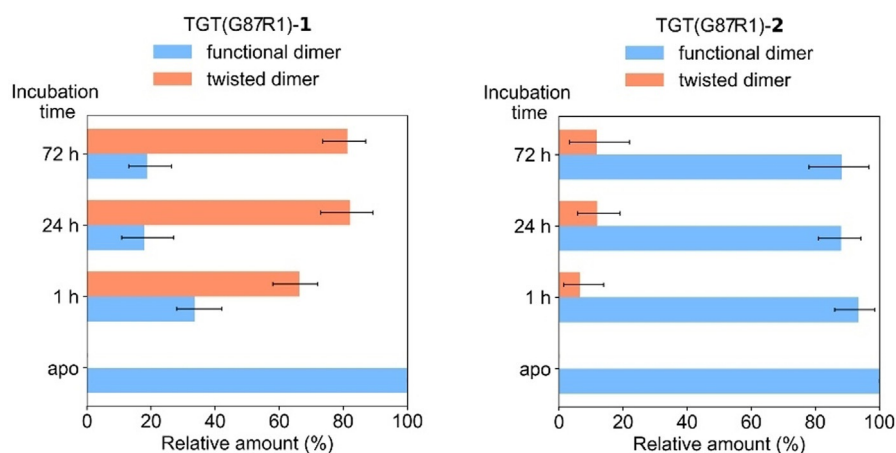

Figure 3. The relative amount of the functional and twisted TGT homodimers in dependence of the incubation time. The error bars are based on Table S6.
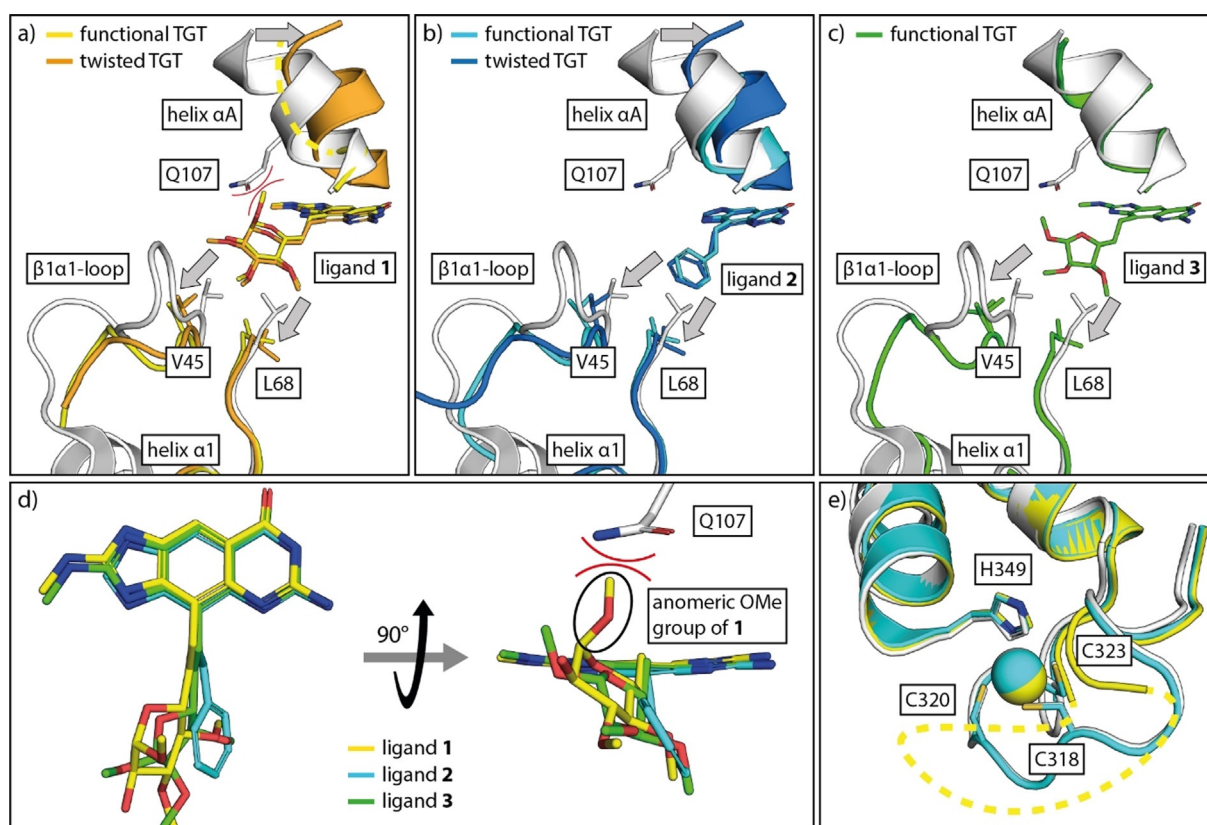
Figure 4. Structural comparison of the functional *apo* TGT structure (gray, PDB-ID 1P0D) with the ligand-bound structures of a) TGT-**1** (functional: yellow, PDB-ID 5LPS; twisted: orange, PDB-ID 5LPT), b) TGT-**2** (functional: cyan, PDB-ID 6YGR; twisted: blue, PDB-ID 5I07), and c) TGT-**3** (functional: green, PDB-ID 5LPO). Structural movements from the functional to the twisted state are indicated by gray arrows. Only one of two equally possible conformations of ligand **1** is shown. Ill-defined residues in TGT-**1** are indicated as yellow dashes. d) Structural comparison of ligands **1**–**3** from their ligand-bound functional dimer structures. The anomeric methoxy group of ligand **1** is encircled in black and its steric conflict with Q107 from *apo* TGT is indicated by red arcs. e) Detailed view of the zinc-binding subdomain of TGT-**1** (yellow) and TGT-**2** (cyan) in the functional dimer form compared to the *apo* structure (gray). Zinc ions are shown as spheres and the zinc-coordinating residues are shown as sticks. Ill-defined residues in TGT-**1** are indicated as yellow dashes.

dimer interface and its ligand-induced destabilization may weaken the formation of the functional homodimer interface.

Previous mass spectrometric studies have revealed that adding ligands to TGT not only results in the crystallographically observed structural rearrangement of the TGT dimer, but also modulates the degree of dissociation.[8,9] Binding of ligands **1**–**3** to TGT(WT) was shown to increase the relative amounts of monomers from 2% to about 10%. In principle, such an increase of the relative amounts of monomers must lead to a decrease of the PELDOR modulation depth parameter λ (Figure 2a) by a factor of ≈ 1.17 i.e., from 0.35 down to 0.30. However, due to uncertainties in the PELDOR background correction and small differences in the pump pulse bandwidth from sample to sample (SI, Chapter 3.4 and Table S5), such a variation in λ is of the same order of magnitude as the experimental error and thus cannot be reliably translated into the monomer-to-dimer ratio. Nevertheless, we tested whether the dimers dissociate into monomers and reassociate to dimers in solution by performing PELDOR experiments on 1:1 mixture of TGT-(WT) homodimers and TGT(G87R1) homodimers equilibrated together for 24 h (Figure S11). If monomers are formed and exchanged between dimers, mixed TGT dimers

containing a TGT(WT) and a TGT(G87R1) monomer should be formed resulting in a reduction of λ compared to the TGT(G87R1) homodimer. Indeed, Figure 5 reveals that λ is reduced to $0.27^{+0.05}_{-0.02}$ for the mixture of TGT(WT) and TGT(G87R1), compared to $0.35^{+0.04}_{-0.06}$ for pure TGT(G87R1).
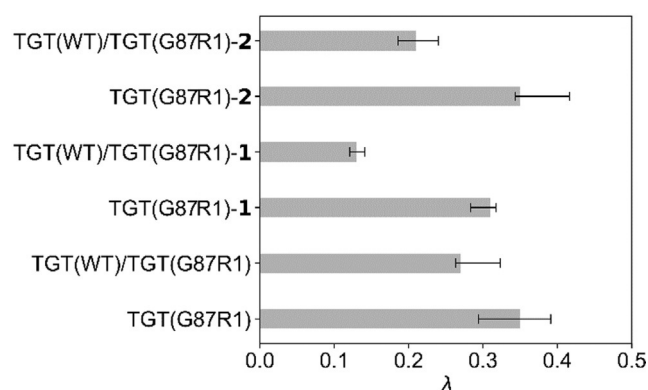

Figure 5. PELDOR modulation depth parameter λ for TGT(G87R1) and the mixture TGT(WT)/TGT(G87R1) without and in presence of ligand **1**. All samples were equilibrated for 24 h. The error bars are based on Table S7.

This suggests that even in the absence of ligands the functional dimers may exchange monomers. However, the uncertainty intervals of both λ values do overlap to some extent cautioning such an interpretation. In contrast, λ of the mixture of TGT(WT) and TGT-(G87R1) is significantly reduced to $0.13^{+0.01}_{-0.01}$ and $0.21^{+0.03}_{-0.02}$ after adding **1** and **2**, compared to $0.31^{+0.01}_{-0.03}$ and $0.35^{+0.07}_{-0.01}$ for the homodimers TGT-(G87R1)-**1** and TGT(G87R1)-**2**, respectively. This reduction in λ is well beyond the uncertainty and indicates that the dissociation into monomers and the formation of mixed dimers is enhanced by binding of **1** and **2**.

A possibility for the reduction in λ could also be that the homodimers are just dissociating to a larger extent into monomers and that no mixed dimers are formed. To shed light on the oligomeric state of the mixed dimers, PELDOR experiments were also carried out on a 1:1 mixture of TGT(G87R1) and TGT(H319R1), equilibrated for 24 h with and without ligand **1** (Figure S12). In the absence of **1**, the distance distribution of the mixture of TGT(G87R1) and TGT-(H319R1) resembles a superposition of the distance distributions of TGT-(G87R1) and TGT(H319R1) homodimers (Figure 6a). However, this result does not exclude the formation of heterodimers because the *MtsslWizard*-based distance prediction shows that the distance distributions for the functional state of the mixed dimer G87R1-H319R1 and the homodimer H319R1-H319R1 cannot be differentiated as they overlap (Figure 6b). In contrast, after equilibrating the mixture of TGT(G87R1) and TGT-(H319R1) with **1**, the distance distribution significantly changes (Figure 6c). In addition to the distance peaks at around 25 Å and 45 Å, which can be assigned to the twisted dimers of TGT(G87R1)-**1** and TGT(H319R1)-**1**, respectively, an additional intense peak at 35 Å appears. Based on comparison with *MtsslWizard* predictions (Figure 6d), this peak can be assigned to the twisted, mixed dimer H319R1-G87R1. Note that the *MtsslWizard*-based prediction of the most probable G87R1-H319R1 distance is slightly larger (≈ 5 Å) than the PELDOR-derived value, but like in the case of the H319R1-H319R1 distance (see above), this difference can be assigned to the error of the *MtsslWizard* prediction. As the distance distributions G87R1-G87R1, G87R1-H319R1, and H319R1-H319R1 significantly overlap, quantification of the relative amount of functional and twisted mixed dimers is not possible.
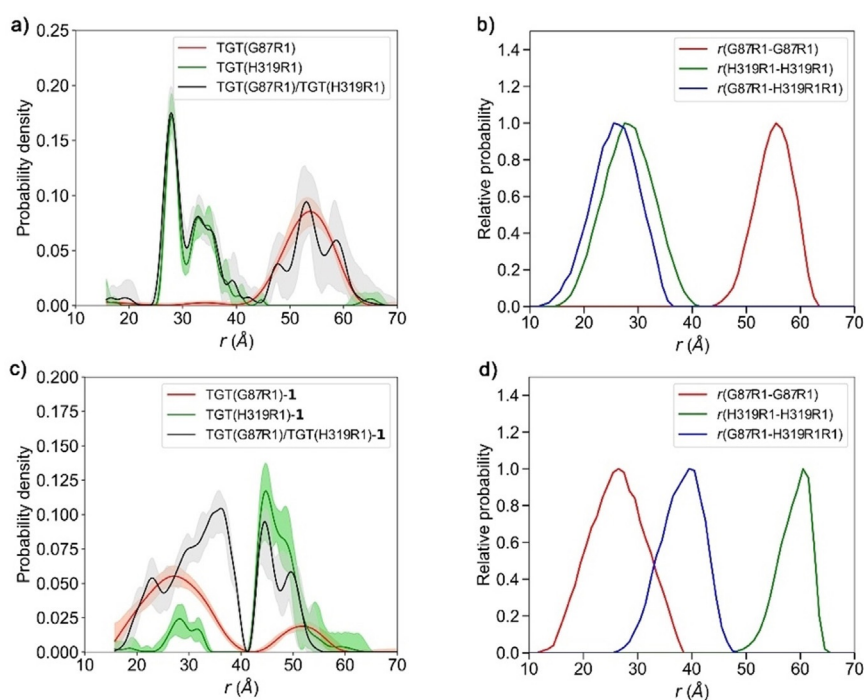

Figure 6. PELDOR measurements on a mixture TGT(G87R1)/TGT(H319R1) without and in presence of ligand **1**. a) PELDOR-based inter-nitroxide distance distributions in TGT(G87R1) (red line), TGT(H319R1) (green line), and TGT(G87R1)/TGT(H319R1) (black line). The corresponding error intervals of the distance distributions are shown as light red, light green, and gray regions, respectively. b) *MtsslWizard*-based predictions of the inter-nitroxide distances G87R1-G87R1 (red line), H319R1-H319R1 (green line), and G87R1-H319R1 (blue line) in functional dimers of TGT(G87R1), TGT(H319R1), and TGT(G87R1)/TGT(H319R1). The *MtsslWizard* models of the spin-labeled mutants were computed using the crystal structure of wild-type TGT (PDB-ID 1P0D). c) PELDOR-based inter-nitroxide distance distributions in TGT(G87R1)-**1** (red line), TGT(H319R1)-**1** (green line), and TGT(G87R1)/TGT(H319R1)-**1** (black line). The corresponding error intervals of the distance distributions are shown as light red, light green, and gray regions, respectively. d) *MtsslWizard*-based predictions of the inter-nitroxide distances G87R1-G87R1 (red line), H319R1-H319R1 (green line), and G87R1-H319R1 (blue line) in twisted dimers of TGT(G87R1)-**1**, TGT(H319R1)-**1**, and TGT(G87R1)/TGT(H319R1)-**1**. The *MtsslWizard* models of the spin-labeled mutants were computed using the crystal structure of TGT-**1** (PDB-ID 5LPT).

Based on the results above, we propose two alternative mechanisms for the ligand-induced structural re-organization of the TGT dimers (Figure 7). The first concerted mechanism is based on the intramolecular rotation of the two monomer units against each other without a significant distal separation of the TGT monomer units. No exchange of monomer units is involved in this mechanism but occurs independently. The second mechanism involves full dissociation of the functional TGT dimer into spatially separated monomers, followed by the re-association of distant monomers into the twisted TGT dimer. Here, the assembly of mutually exchanged monomer units is possible and even likely. Formally, the present experiments cannot differentiate between these two extremes. First of all, the concerted mechanism passes through a small separation of the monomer units, whereas the dissociation–association mechanism requires a large splitting of them. Thus, any differentiation of both mechanisms will depend on a predefined distance threshold which will be difficult to set. Nevertheless, since the process is extremely slow and needs hours to be accomplished, the second
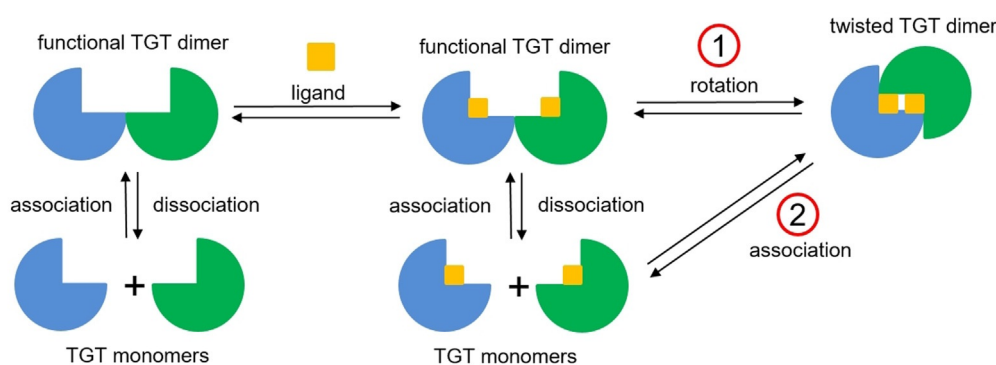
Figure 7. Two possible mechanisms of structural re-organization of the functional TGT homodimer into the twisted TGT homodimer.

mechanism appears more likely. In addition, the dissociation and re-association of the ligand-free functional dimer only speaks for this mechanism. Furthermore, the kinetics of the two mechanistic extremes should differ in their concentration dependence but may be overlaid. If the concerted mechanism would be in operation, an explanation must be given, why the probability rate of the monomer rotation is so small. The barrier must be extremely high and even increases for the ligand-free case. Further investigations and computer simulations are needed to address the mechanistic issue in the future.

Conclusion

In this study, we designed an EPR-based approach to uncover the formation of the twisted TGT dimer in a solution equilibrium. Promising spin-labeling sites were evaluated *in silico* and two spin-labeled mutants, TGT(G87R1) and TGT-(H319R1), were designed. The PELDOR distance distributions fit well with the predicted distances from previously obtained crystal structures, thus verifying that the twisted dimer exists as a species in solution and is not imposed by crystal packing forces. Only with ligand **1** or **2**, the two separated species can be recorded by PELDOR. While for **1** the twisted form is populated to about 80%, **2** only marginally shows the transformed twisted state to about 10% besides the higher populated functional dimer. Since the PELDOR experiments were performed on flash-frozen samples after incubation at room temperature, a shift in the equilibrium between the functional and twisted dimer states during the freezing process cannot be ruled out.

We hypothesize that a small structural detail of ligand **1**, the anomeric methoxy group at its pyranose substituent, is able to displace the nearby helix αA and thereby favors the enhanced rearrangement into the higher populated twisted dimer along with perturbations of the loop-helix motif. Ligands with substituents occupying a similar or even larger space as this methoxy group might be worth for further investigations.

Based on the PELDOR results, we suggest a mechanism for the formation of the TGT twisted dimer based on dissociation of the dimers into monomers and their statistical reassociation into the twisted or functional state.

Conflict of Interest

The authors declare no conflict of interest.

[1] H. Nishi, K. Hashimoto, T. Madej, A. R. Panchenko, *Prog. Mol. Biol. Transl. Sci.* **2013**, *117*, 3–24.

[2] K. Hashimoto, H. Nishi, S. Bryant, A. R. Panchenko, *Phys. Biol.* **2011**, *8*, 035007.

[3] G. G. Hammes, C. W. Wu, *Science* **1971**, *172*, 1205–1211.

[4] N. Shimba, A. M. Nomura, A. B. Marnett, C. S. Craik, *J. Virol.* **2004**, *78*, 6657–6665.

[5] T. Shahian, G. M. Lee, A. Lazic, L. A. Arnold, P. Velusamy, C. M. Roels, R. K. Guy, C. S. Craik, *Nat. Chem. Biol.* **2009**, *5*, 640–646.

[6] T. H. Tran, P. Alexander, S. Dharmaiah, C. Agamasu, D. V. Nissley, F. McCormick, D. Esposito, D. K. Simanshu, A. G. Stephen, T. E. Balius, *Proc. Natl. Acad. Sci. USA* **2020**, *117*, 3363–3364.

[7] S.-M. Lin, S.-C. Lin, J.-N. Hsu, C.-K. Chang, C.-M. Chien, Y.-S. Wang, H.-Y. Wu, U.-S. Jeng, K. Kehn-Hall, M.-H. Hou, *J. Med. Chem.* **2020**, *63*, 3131–3141.

[8] F. R. Ehrmann, J. Stojko, A. Metz, F. Debaene, L. J. Barandun, A. Heine, F. Diederich, S. Cianférani, K. Reuter, G. Klebe, *PLoS One* **2017**, *12*, e0175723.

[9] F. R. Ehrmann, J. Kalim, T. Pfaffeneder, B. Bernet, C. Hohn, E. Schäfer, T. Botzanowski, S. Cianférani, A. Heine, K. Reuter, F. Diederich, G. Klebe, *Angew. Chem. Int. Ed.* **2018**, *57*, 10085–10090; *Angew. Chem.* **2018**, *130*, 10242–10247.

[10] W. Xie, X. Liu, R. H. Huang, *Nat. Struct. Biol.* **2003**, *10*, 781–788.

[11] T. Ritschel, C. Atmanene, K. Reuter, A. van Dorsselaer, S. Sanglier-Cianferani, G. Klebe, *J. Mol. Biol.* **2009**, *393*, 833–847.

[12] A. D. Milov, K. M. Salikhov, M. D. Shchirov, *Sov. Phys. Solid State* **1981**, *23*, 565–569.

[13] R. E. Martin, M. Pannier, F. Diederich, V. Gramlich, M. Hubrich, H. W. Spiess, *Angew. Chem. Int. Ed.* **1998**, *37*, 2833–2837; *Angew. Chem.* **1998**, *110*, 2993–2998.

[14] K. J. Oh, H. Zhan, C. Cui, K. Hideg, R. J. Collier, W. L. Hubbell, *Science* **1996**, *273*, 810–812.

[15] T. Hett, T. Zbik, S. Mukherjee, H. Matsuoka, W. Bönigk, D. Klose, C. Rouillon, N. Brenner, S. Peuker, R. Klement, H.-J. Steinhoff, H. Grubmüller, R. Seifert, O. Schiemann, U. B. Kaupp, *J. Am. Chem. Soc.* **2021**, *143*, 6981–6989.

[16] A. Collauto, H. A. DeBerg, R. Kaufmann, W. N. Zagotta, S. Stoll, D. Goldfarb, *Phys. Chem. Chem. Phys.* **2017**, *19*, 15324–15334.

[17] K. Barth, S. Hank, P. E. Spindler, T. F. Prisner, R. Tampé, B. Joseph, *J. Am. Chem. Soc.* **2018**, *140*, 4527–4533.

[18] R. Dastvan, S. Mishra, Y. B. Peskova, R. K. Nakamoto, H. S. Mchaourab, *Science* **2019**, *364*, 689–692.

[19] C. A. J. Hutter, M. H. Timachi, L. M. Hürlimann, I. Zimmermann, P. Egloff, H. Göddeke, S. Kucher, S. Štefanić, M. Karttunen, L. V. Schäfer, E. Bordignon, M. A. Seeger, *Nat. Commun.* **2019**, *10*, 2260.

[20] M. F. Peter, A. Tuukkanen, C. A. Heubach, A. Selsam, F. G. Duthie, D. Svergun, O. Schiemann, G. Hagelueken, *Structure* **2019**, *27*, 1416.

[21] O. Duss, E. Michel, M. Yulikov, M. Schubert, G. Jeschke, F. H. Allain, *Nature* **2014**, *509*, 588–592.

[22] L. J. Berliner, J. Grunwald, H. Hankovszky, K. Hideg, *Anal. Biochem.* **1982**, *119*, 450–455.

[23] G. Likhtenshtein, J. Yamauchi, S. Nakatsuji, A. I. Smirnov, R. Tamura, *Nitroxides: Applications in Chemistry, Biomedicine, and Materials Science*, Wiley-VCH, Hoboken, **2008**.

[24] L. Fábregas Ibáñez, G. Jeschke, S. Stoll, *Magn. Reson.* **2020**, *1*, 209–224.

[25] S. G. Worswick, J. A. Spencer, G. Jeschke, I. Kuprov, *Sci. Adv.* **2018**, *4*, eaat5218.

[26] G. Jeschke, V. Chechik, P. Ionita, A. Godt, *Appl. Magn. Reson.* **2006**, *30*, 473–498.

[27] R. A. Stein, A. H. Beth, E. J. Hustedt, *Methods Enzymol.* **2015**, *563*, 531–567.

[28] J. P. Klare, *Biol. Chem.* **2013**, *394*, 1281–1300.

[29] O. Schiemann, T. F. Prisner, *Q. Rev. Biophys.* **2007**, *40*, 1–53.

[30] G. W. Reginsson, O. Schiemann, *Biochem. J.* **2011**, *434*, 353–363.

[31] G. Jeschke, *Annu. Rev. Phys. Chem.* **2012**, *63*, 419–446.

[32] G. Hagelueken, D. Abdullin, O. Schiemann, *Methods Enzymol.* **2015**, *563*, 595–622.